Received: 11 June 2018 | Accepted: 21 August 2018

DOI: 10.1111/bcpt.13119

ORIGINAL ARTICLE

BCPT Basic & Clinical Pharmacology & Toxicology

Physicochemical predictors of Multi-Walled Carbon Nanotube–induced pulmonary histopathology and toxicity one year after pulmonary deposition of 11 different Multi-Walled Carbon Nanotubes in mice

Kristina B. Knudsen[1] | Trine Berthing[1] | Petra Jackson[1] | Sarah S. Poulsen[1] | Alicja Mortensen[1] | Nicklas R. Jacobsen[1] | Vidar Skaug[2] | Józef Szarek[3] | Karin S. Hougaard[1] | Henrik Wolff[4] | Håkan Wallin[2] | Ulla Vogel[1,5]

[1]National Research Centre for the Working Environment, Copenhagen Ø, Denmark

[2]National Institute of Occupational Health, Oslo, Norway

[3]Department of Pathophysiology, Forensic Veterinary Medicine and Administration, University of Warmia and Mazury in Olsztyn, Olsztyn, Poland

[4]Finnish Institute of Occupational Health, Helsinki, Finland

[5]Department of Micro- and Nanotechnology, DTU, Lyngby, Denmark

Correspondence
Ulla Vogel, National Research Centre for the Working Environment, Copenhagen Ø, Denmark.
Email: ubv@nrcwe.dk

Funding information
The project was supported by Danish Center for Nanosafety, grant # 20110092173-3 from the Danish Working Environment Research Foundation, Danish Centre for Nanosafety II, the European Union under grant agreements #310584 [NANoREG], and # 686098 [SmartNanoTox] and by the Danish Council of Independent Research (Medical Sciences, grant No. 6110-00103).

Abstract

Multi-walled carbon nanotubes (MWCNT) are widely used nanomaterials that cause pulmonary toxicity upon inhalation. The physicochemical properties of MWCNT vary greatly, which makes general safety evaluation challenging to conduct. Identification of the toxicity-inducing physicochemical properties of MWCNT is therefore of great importance. We have evaluated histological changes in lung tissue 1 year after a single intratracheal instillation of 11 well-characterized MWCNT in female C57BL/6N BomTac mice. Genotoxicity in liver and spleen was evaluated by the comet assay. The dose of 54 μg MWCNT corresponds to three times the estimated dose accumulated during a work life at a NIOSH recommended exposure limit (0.001 mg/m^3). Short and thin MWCNT were observed as agglomerates in lung tissue 1 year after exposure, whereas thicker and longer MWCNT were detected as single fibres, suggesting biopersistence of both types of MWCNT. The thin and entangled MWCNT induced varying degree of pulmonary inflammation, in terms of lymphocytic aggregates, granulomas and macrophage infiltration, whereas two thick and straight MWCNT did not. By multiple regression analysis, larger diameter and higher content of iron predicted less histopathological changes, whereas higher cobalt content significantly predicted more histopathological changes. No MWCNT-related fibrosis or tumours in the lungs or pleura was found. One thin and entangled MWCNT induced increased levels of DNA strand breaks in liver; however, no physicochemical properties could be related to genotoxicity. This study reveals

Abbreviations: Al, aluminium; BET, specific surface area; CNT, carbon nanotubes; Co, cobalt; COOH, carboxylation; ELISA, the enzyme-linked immunosorbent assay; Fe, iron; H&E, haematoxylin and eosin; HARN, high aspect ratio nanomaterials; I.T., intratracheal; IARC, International Agency for Research on Cancer; IP, intraperitoneal; LOAEL, lower observed adverse effect level; Mg, magnesium; Mn, manganese; MWCNT, multi-walled carbon nanotubes; Ni, nickel; NOAEL, no observed adverse effect level; OECD, Organisation for Economic Co-operation and Development; OH, hydroxylation; ROS, reactive oxygen species; SAA, serum amyloid A; SD, standard deviation; WPMN, Working Party on Manufactured Nanomaterials.

physicochemical-dependent difference in MWCNT-induced long-term, pulmonary histopathological changes. Identification of diameter size and cobalt content as important for MWCNT toxicity provides clues for designing MWCNT, which cause reduced human health effects following pulmonary exposure.

KEYWORDS

biodistribution, carbon nanotubes, granuloma, in vivo, lymphocytic aggregate, macrophage infiltration

1 | INTRODUCTION

High aspect ratio nanomaterials (HARN) are under scientific awareness due to the known occupational and public health problems caused by the inhalation of asbestos fibres.[1] The physical aspects of multi-walled carbon nanotubes (MWCNT) ensure their inclusion as HARN; however, as group, MWCNT still differ vastly in physicochemical properties. This includes length, thickness, structure, metal impurities and surface modifications.[2] MWCNT are used in a wide variety of applications, resulting in possible human exposure.[3-5] Identification of the toxicity-driving physicochemical properties of MWCNT is therefore of great importance for regulatory purposes and as well as for safe-by-design, which is design of MWCNT to reduce toxicity without losing desirable properties. However, before fully achieving this goal lays a comprehensive task. Completing this task will require studies with long-term exposure scenarios, inclusion of a broad variety of MWCNT, comparable and relevant dosing, and thorough physicochemical characterization. In the present study, these aspects are taken into account.

MWCNT toxicity has been extensively studied in the last decade, but the majority of these studies have been acute or sub-acute studies comprising one or few MWCNT. The main findings from these studies were a general MWCNT-induced inflammatory response and inflammation-related changes in the lung after pulmonary exposure.[6-9] The potency of the observed inflammatory responses differed across MWCNT types relative to their physicochemical properties.[10-14] Some MWCNT induced fibrosis or changes related to fibrosis, but these changes were largely dose-dependent.[14-18] In addition, increased plaque progression, increased blood levels of proteins related to plaque progression and changes in secondary organs such as the liver have also been reported after pulmonary exposure to MWCNT.[19-23] However, in order to identify persistent pathological changes, long-term studies are needed. Three sub-chronic inhalation studies investigating different short (1-10 μm) and thin (~10 nm) MWCNT reported pulmonary inflammation in rats that persisted until the latest follow-up time of 26 weeks after exposure.[24-26] Moreover, dose-dependent fibrosis was identified in two of the three studies. In the other end of the physical spectrum, the long (>5 μm), thick (~90 nm) and rigid MWCNT type called XNRI-7 was recently reported to induce dose-dependent inflammation and focal fibrosis in rats in a pivotal 2-year inhalation study.[17] XNRI-7 is also called MWNT-7, Mitsui-7 and NRCWE 006 and was produced by the Japanese company Mitsui. It is the most well-studied MWCNT in the literature. In addition, XNRI-7/MWNT-7 exposure also induced lung carcinogenicity and pleural focal fibrosis, whereas no pleural mesotheliomas were observed. MWCNT with similar dimensions as XNRI-7/MWNT-7 induced both pleural malignant mesothelioma and lung tumours after intratracheal instillation in rats.[27] Correspondingly, a 2-year study using intrapleural injection showed that four different long, thick and needlelike MWCNT induced cancer,[28] whereas short and thin MWCNT did not.[29] This highlights the possible carcinogenicity of the more needlelike MWCNT, which ultimately have resulted in XNRI-7/MWNT-7 being classified as possibly carcinogenic to humans by IARC.[30]

The aim of this study was to investigate toxicological changes one year after single intratracheal administration of 11 different MWCNT in mice at a dose of 54 μg/mouse. The tested MWCNT included XNRI-7/MWNT-7, four OECD standard MWCNT, and two sets of functionalized MWCNT (pristine, hydroxylated, carboxylated). The portfolio of MWCNT was selected to include a broad variety of physicochemical properties: a set of thin and entangled, a set of longer and needlelike, and a set of surface modified vs pristine MWCNT. Several of these MWCNT have previously been included in our 90-day studies,[13,19] thus enabling comparison across time-points. These studies used the same route of exposure as in the present study, and they investigated physicochemical determinants of more acute toxicological effects in terms of pulmonary neutrophil influx, genotoxicity and induction of the acute phase response. In this work, we extend the follow-up period to one year to gain a better understanding of the long-term outcome and relevance of lesions following exposure to MWCNT. Our primary end-points were pulmonary histopathological changes and genotoxicity in spleen and liver. However, other systemic end-points were also investigated. Primary end-points were correlated to the physicochemical properties of the studied MWCNT by multiple regression analysis, in order to identify specific properties important for long-term MWCNT-induced toxicity.

Inhalation studies are the gold standard of toxicity testing, but the deposited pulmonary dose can be difficult to monitor due to differences in sizes of the aerosolized particle agglomerates, resulting in differences in deposition.[31] In the present study, intratracheal instillation was chosen as exposure route. Aspiration[32-34] and intratracheal instillation[14,35,36] are widely used in screening studies, with accurate dose delivery, allowing for comparison of toxicity between test materials.[20,37,38] The chosen dose corresponds to three times the estimated life-time deposited dose in humans at the suggested occupational exposure limit of 0.001 mg/m^3,[39] assuming a pulmonary deposition of 10%,[24] a 40-h working week during 40 years, while ignoring pulmonary clearance. The dose is relevant for occupational exposure and lower than the doses used in most studies. However, as the dose is delivered as a bolus, the dose rate is much higher than in inhalation studies and in occupational settings. Studies using instillation as exposure route are therefore useful for quantitative hazard ranking, but not for quantitative risk assessment.[40]

Direct comparison of results across animal studies can be troublesome, as protocols often differ between laboratories with regard to exposure methods, doses, animals and strains, and time periods. With the choices of MWCNT and experimental set-up in the present study, such interferences were minimized, thus making true differences more readily detected.

2 | METHODS

2.1 | Materials

Eleven multi-walled carbon nanotubes (MWCNT) were analysed. As well-studied benchmark materials, we included MWCNT from the OECD's Working Party on Manufactured Nanomaterials (WPMN) (NM-400, NM-401, NM-402, NM-403). We also included the MWCNT XNRI-7/MWNT-7, a kind gift from Mitsui (Lot# 05072001K28; Tokyo, Japan), coded as NRCWE-006. Finally, six MWCNT were purchased from Cheap Tubes (Brattleboro, VT, USA), NRCWE-040 to NRCWE-048 (group I and III in[2]), as two pristine and four functionalized MWCNT (-OH and -COOH). Carbon black Printex 90, a kind gift from Degussa-Hüls (Frankfurt, Germany), was included as reference material. All nanomaterials were thoroughly characterized in house,[2] data were published previously and are summarized in Table 1 and in Tables S1 and S2.

2.2 | Material dispersion

Nanomaterial dispersions were prepared as previously described.[14] The MWCNT stock dispersions were prepared in a concentration of 2.56 mg/mL in 0.45-μm MilliQ filtered Nanopure water with 2% mouse serum. Printex 90 dispersion was prepared as in previous studies for comparison,[41-43] in a stock of 3.24 mg/mL in 0.45-μm MilliQ filtered Nanopure water. Dispersions were sonicated in a volume of 4-6 mL for 16 min. using a 400 W Branson Sonifier S-450D (Branson Ultrasonics Corp., Danbury, CT, USA) mounted with a disruptor horn and operated at 10% amplitude. The dispersions were continuously cooled by ice/water. The dilution used for instillation was prepared directly after sonication and was further sonicated for 2 min. after re-suspension.

2.3 | Animals

A total of 150 female mice C57BL/6N BomTac aged 7 - 8 weeks (average weight 18.6 ± 1.1 g) were obtained from Taconic Europe (Ejby, Denmark). Mice were allocated arbitrarily to the experimental groups and were acclimatized for 1 week before the start of experiment. The mice were housed in groups of 5 animals in each polypropylene cage with bedding (sawdust) and enrichment at controlled environmental conditions: temperature (21 ± 1°C), humidity (50% ± 10%) and 12-hr light/dark period. Mice had access to food (Altromin 1324) and tap water ad libitum as previously described.[41]

2.4 | Study design

The female C57BL/6N BomTac mice were dosed by a single intratracheal instillation of 54 μg/mouse at 8-9 weeks of age. Ten mice were included per MWCNT and Printex 90 group and 30 mice for the vehicle control group. Mice were weighed at the day of the intratracheal instillation, two days post-instillation and monthly until 1 year post-exposure where the study was terminated. Mice instilled with Printex 90 received 162 μg/mouse, a reference dose observed to induce inflammation and genotoxicity in our previous studies.[13,14,35,37,38,41,44,45] During the post-exposure observation period, eight mice were euthanized due to bad health unrelated to the MWCNT exposure, due to infected wounds inflicted by biting or due to excessive grooming (one mouse from groups NM-401, NM-403, NRCWE-006, Printex-90, NRCWE-042, NRCWE-047 and two vehicle controls). The organs from the mice, which were removed from the study after month eleven, were collected and evaluated along with the rest. One year post-exposure, mice were killed, and lung, heart, liver, kidney, spleen, diaphragm, chest wall, mediastinal lymph nodes and brains were collected. All procedures complied with the EC Directive 86/609/EEC and Danish law regulating experiments with animals (The Danish Ministry of Justice, Animal Experiments Inspectorate, permission 2006/561-1123).

2.5 | Instillation

Mice were instilled intratracheally as described previously.[46,47] Briefly, mice were anaesthetized using isoflurane

TABLE 1 Physicochemical characteristics of MWCNT

MWCNT	Type	Manufacturer/distributor	Product code	Carbon[a] (%)	Length[b] (µm)	Diameter[b] (nm)	BET[c] (m^2/g)	CEA:O[d] mmol/g	OH[e] $mmol/m^2$	COOH[e] $mmol/m^2$
NM-400	Pristine	OECD WPMNM	JRCNM04000a	94.8	0.85 ± 0.10	11 ± 3	254	0.81 ± 0.02	0.0032	0.0016
NM-401	Pristine	OECD WPMNM	JRCNM04001a	99.7	4.0 ± 0.37	67 ± 24	18	0.03 ± 0.001	0.0017	0.0011
NM-402	Pristine	OECD WPMNM	JRCNM04002a	96.1	1.4 ± 0.19	11 ± 3	226	0.28 ± 0.01	0.0012	0.0006
NM-403	Pristine	OECD WPMNM	JRCNM04003a	99.1	0.4 ± 0.03	12 ± 7	135	0.19 ± 0.01	0.0014	0.0007
NRCWE-006	Pristine	Mitsui/Hadogaya	XNRI MWNT-7	99.6	5.7 ± 0.49	74 (29-173)	26	0.08 ± 0.003	0.0031	0.0015
NRCWE-040	Pristine	Cheaptubes	sku-030102	98.6	0.52 ± 0.59	20.56 ± 6.9	150	0.35 ± 0.01	0.0023	0.0012
NRCWE-041	OH	Cheaptubes	sku-030202	99.2	1.0 ± 2.95	26.38 ± 11.1	152	1.69 ± 0.07	0.011	0.0056
NRCWE-042	COOH	Cheaptubes	sku 030302	99.2	0.72 ± 0.97	20.5 ± 5.32	141	4.09 ± 0.20	0.029	**0.0069**
NRCWE-046	Pristine	Cheaptubes	sku-030111	98.7	0.72 ± 1.2	17.2 ± 5.8	223	0.63 ± 0.03	0.0028	0.0014
NRCWE-047	OH	Cheaptubes	sku 030112	98.7	0.53 ± 0.59	12.96 ± 4.4	216	0.26 ± 0.01	0.0012	0.0006
NRCWE-048	COOH	Cheaptubes	sku 030113	98.8	1.6 ± 5.6	15.08 ± 4.7	185	0.58 ± 0.02	0.0031	**0.0012**
Carbon black	-	Evonik	Printex 90	99.3	-	9	182	1.45 ± 0.03		

Notes. Further physicochemical characteristics published in Jackson et al[2] and Poulsen et al[13] and included in Tables S1 and S2.

[a]Carbon weight percent determined by wavelength dispersive X-ray fluorescence spectrometry. [b]Dimensions ± standard deviation (SD) determined by computerized image analysis of SEM micrographs. [c]Brunauer-Emmett-Teller (BET) analysis of specific surface area. [d]Total content of oxygen ± ~95% confidence limits, measured by combustion elemental analysis (CEA). The 95% confidence limits are based on the expanded uncertainty of the method and a coverage factor of 2. [e]Surface density calculated by assuming that all oxygen measured by CEA was OH- or COOH-group and dividing by surface area (BET). COOH surface densities in bold are based on acid-base titrations (Jackson et al[2]).

with 4-5% of oxygen with a flow of 80% in the chamber until fully relaxed. A 50 μL suspension was instilled followed by 200 μL air with a 250-μL SGE glass syringe (250F-LT-GT, Micro-Lab, Aarhus, Denmark). After the procedure, each mouse was weighed and after full recovery it was transferred to the animal facility. The average weight at instillation was 18.6 ± 1.1 g.

2.6 | Open-field behaviour

The animals were tested in the open-field test eleven months post-exposure to assess anxiety-like behaviour. Animals were transferred to the experimental room 1 hr before the first test, during the animals' light period. Exposed and control animals were tested blinded to their exposure status. Activity was monitored for 3 min. in a circular, white, open field (∅100 cm) as described in[47] with minor modifications. Trials commenced in the centre of the field and were registered by Noldus Ethovision (Version 5, Noldus Information Technology, Wageningen, the Netherlands) that also calculated total ambulation, which was split into three time bins of 1 min to test for habituation. Duration in the central and peripheral zone of the field, as well as the number of crossings from the outer to the central zone, was extracted.

2.7 | Necropsy

On the day of necropsy, mice were weighed and then anaesthetized by an I.P. injection with ZRF cocktail (Zoletil Forte 250 mg, Rompun 20 mg/mL, Fentanyl 50 μg/mL in sterile isotone saline, dose 0.1 mL/25 g body-weight). Heart blood was withdrawn and stabilized with K_2EDTA. Lungs were filled slowly with 4% formalin under 30-cm water column pressure in situ. A knot was made around the trachea to secure formalin in lungs to fixate tissue in "inflated state." Lungs were then removed from the chest cavity, along with the heart, liver, kidney, spleen, diaphragm, a piece of right lower chest wall and mediastinal lymph nodes and placed in 4% formalin for 24 hr. Brains were also removed and snap-frozen in liquid nitrogen along with a piece from kidney, spleen and liver used for genotoxicity testing. The brains and kidneys were not analysed in this study.

2.8 | Histology and imaging

The formalin-fixed tissue samples from the collected organs (lung, heart, liver, kidney, spleen, diaphragm, chest wall and mediastinal lymph nodes) were trimmed, dehydrated on a Leica ASP300S (Leica Systems, Wetzlar, Germany) and embedded in paraffin. Heart, liver, kidney and spleen were not evaluated in this study. Sections were cut at 3 μm on a Microm HM 355S Microtome (Thermo Scientific™, East Windsor, New Jersey, USA). Sections for light microscopic examinations were stained with Haematoxylin and Eosin (H&E- staining) or Sirius Red staining. The sections were examined by light microscopy performed with a Nikon Eclipse E 800 microscope and an Olympus BX43 microscope. Images were acquired at 10×, 40× and 100× on an Olympus BX 43 microscope with a Qimaging Retiga4000R camera. Uneven illumination in brightfield images was corrected using ImageJ[48] and the Calculator Plus plugin via the formula: Corrected_image = (Image/background) * 255. The background image was a maximum projection of 3 background brightfield images without tissue. Images of entire lung sections were made by acquiring multiple overlapping images at 10x. Images were assembled in ImageJ using MosaicJ plugin.[49]

Cytoviva enhanced darkfield hyperspectral system (Auburn, AL, USA) was used to detect single CNTs, by carefully scanning lung and liver sections at 40× in enhanced darkfield mode. Darkfield images of single CNTs were acquired at 100×.

2.9 | Histopathology

Lymphocytic aggregates, granulomas and macrophage infiltrates in lungs were scored essentially as described in Poulsen et al[13] (Table 2). For each scored entity, the scoring was performed on the lung lobe with the most histopathological changes, which most often was the left lung lobe. General examples of histological changes are shown in Figure 1. Granulomas were defined as foreign body granulomas with material surrounded entirely by adherent macrophages as seen in Figure 1Ai. Macrophage infiltrates refer to focally increased concentrations of macrophages with or without ingested CNTs. A macrophage infiltrate is shown in Figure 1Aii. For the lymphocytic aggregates, the majority of the cells are lymphocytes with hyperchromatic nuclei and scant cytoplasm (Figure 1Aiii). Alveolar interstitial fibrosis (excluding perivascular and peribronchiolar

TABLE 2 Scoring system for histological changes in lung

Score	Lymphocytic aggregates	Granulomas	Macrophage infiltrates
0	None	None	None
1	1 aggregate	1-2 granulomas	Any infiltrate
2	2-3	3-4	Infiltrate > 10% of section
3	4-6	5-8	>20% of section
4	7-10	9-16	>30% of section
5	>10	>16	>50% of section

Note. Scoring was performed on the lung lobe containing most changes for each animal.

collagen (Figure S1C) and collagen around granulomas), pleural fibrosis and tumours, were noted, but not scored as these were infrequent and very localized findings.

The grading of pulmonary lymphocytic and macrophage infiltration in the exposure groups was compared to the control group by one-way ANOVA with a post hoc Dunnett's comparison test. Differences between MWCNT exposure groups were tested by one-way ANOVA using Bonferroni correction for multiple testing. Granuloma formation, fibrosis and tumour incidence in lungs were compared to control group with Fisher's exact test using Bonferroni correction for multiple testing. $P < 0.05$ was considered significant.

2.10 | Serum amyloid levels in plasma

Levels of SAA3 in plasma were measured by sandwich ELISA from EMD Millipore (Cat. # EZMSAA#-12K) as described in[20]. Samples were analysed according to the manufacturer's protocol. Shortly, mouse SAA3 from plasma samples was captured in microtitre plates pre-coated with anti-Mouse SAA3 polyclonal antibody. Unbound material was washed away, and biotinylated anti-Mouse SAA3 polyclonal antibody was attached. Samples were washed again, and horseradish peroxidase was conjugated to the immobilized biotinylated antibody. Washed samples were analysed by spectrophotometry to quantify the horseradish peroxidase activity in the presence of substrate 3,3',5,5'-tetramethylbenzidine. Increase in absorbance is proportional to the amount of captured SAA3.

2.11 | Analysis of DNA strand break levels by comet assay

DNA strand break levels were analysed by the comet assay described previously by Jackson et al.[50] DNA strand breaks were determined on frozen liver tissue (3 × 3 mm piece of median lobe) and spleen (3 × 3 mm piece). Frozen tissues were homogenized in Merchant's medium. Cells were suspended in agarose at 37°C with final agarose concentration of 0.7% and then embedded on Trevigen CometSlides™ (30 μL per well for a 20-well slide). Cooled slides were placed in lysis buffer overnight at 4°C. The next day, slides were rinsed in electrophoresis buffer, alkaline-treated for 40 min., and electrophoresis was run for 25 min. at 1.15V/cm (38V). Slides were neutralized (2 × 5 min.), fixed in ethanol for 5 min. and placed on a warm plate at 45°C for 15 min. Cells were stained with TE-buffered SYBR®Green fluorescent stain for 30 min., dried at 37°C for 10 min., UV filter and coverslip were applied, and DNA damage was analysed by IMSTAR Pathfinder™ system. Related samples were placed in the same electrophoresis. The results are presented as average %TDNA value for all cells scored on each Trevigen CometSlide well. The day-to-day variation and electrophoresis efficiency were validated by including PBS exposed and 60 μM H_2O_2-exposed A549 cells as negative and positive controls, respectively, on each slide. Control cells were exposed for 30 min. at 4°C as described in.[50] The slide-to-slide variation including all slides (n = 8) from this experiment was %TDNA 18.3%. %TDNA and tail length (TL) in liver and spleen for control group were compared to exposed groups using a parametric one-way ANOVA with a post hoc Tukey-type experimental comparison test in SAS version 9.3 (SAS Institute Inc., Cary, NC, USA). The data were log-transformed to reach parametric requirements.

2.12 | Multiple regression analyses

Chosen variables for the multiple regression and logistic regression analyses included: BET surface area, Fe, Mn, Ni, Co, Mg, the diameters, the lengths and OH. Aluminium was omitted due to missing values for several MWCNT. As described previously, functionalizations were calculated under the assumption that all oxygen atoms were either OH or COOH, respectively.[2] Oxygen content as OH-functionalization was therefore chosen as the regression variable in the further analyses. All covariates, except BET surface area, were log-transformed using base 2. For BET surface area, we used log(BET)/log(1.25). If possible, the detection limit for the chemical composition was imputed when values were below the detection limit (underdetect values). We included indicator variables for below detection limit to ensure that the imputed values did not affect the estimated association between the outcome and the chemical composition. For the multiple logistic regression analyses, problematic underdetect values were identified using 2 × 2 cross tables. If the variables' relationship with the outcome relied completely on the underdetect variable, then this, and hence the MWCNT type, was removed from the specific analysis.

Initially, we investigated the pairwise associations between physicochemical parameters (BET surface area, Fe, Mn, Ni, Co, Mg, diameter, length and functionalization) in Pearson's correlation analysis (Table S9). Two clusters of highly correlated parameters were observed: Cluster 1 included BET surface area, diameter and length. Cluster 2 included Mn, Mg, Co and Fe (Table S9). Separation of the effects of these parameters in the clusters is questionable. Additionally, Ni was included in cluster 1 due to their covariance with some, but not all, parameters in the clusters (Table S9). For cluster 1, we chose to use diameter (log-transformed) as the proxy variable in the multiple regression and multiple logistic regression analyses, as this diameter displayed good tolerance and explained most of the variance when compared to the other variables of cluster 1. We also present the results using log-transformed length as the proxy variable (Tables S10 and

S11), as length, compared to diameter, was an equally strong predictor for the end-points (results not shown). For cluster 2, we chose Fe (log-transformed) as the proxy variable in the multiple regression and multiple logistic regression analyses, as Fe displayed good tolerance and explained most of the variance when compared to the other variables of cluster 2. However, the results using log-transformed Mn is also presented in Tables S11 and S12, as Mn and Fe were equally strong predictors for the end-points (results not shown). Oxygen content was the only independent variable.

Multiple regression was performed with lymphocytic infiltration as outcome, as almost all observations included lymphocytic infiltration of various scores. Similarly, multiple regression analyses were performed on the hepatic %TDNA data, as the data were in the numerical scale. Multiple logistic regression was performed with macrophage infiltration and granuloma formation as outcome, as these observations could be divided into either containing the outcome or not. All correlations, multiple regression and multiple logistic regression analyses were performed in SAS version 9.3 (SAS Institute Inc.). Statistical significance was determined at the 0.01 level in the multiple regression and multiple logistic regression analyses, since several analyses (8 per outcome) were performed with no other correction for mass significance.

3 | RESULTS

3.1 | Material characterization

Data on the physicochemical properties of the MWCNT have previously been reported in detail (Table 1 and Tables S1 and S2).[2] The MWCNT include four OECD standard materials (NM-400 to -403) and XNRI-7/MWNT-7, named NRCWE-006 in this study. In addition, two groups of functionalized MWCNT were included. These groups comprised pristine, hydroxylated and carboxylated MWCNT. Analyses identified NM-401 and NRCWE-006 as thick, long, and needlelike with low levels of metal contamination, whereas NM-400, NM-402, NM-403 and NRCWE-040-48 were considerably shorter and thinner and appeared entangled. NRCWE-041 and NRCWE-042 had increased total oxygen content compared to the pristine NRCWE-040. For NRCWE-042, titration analysis indicated that half of the oxygen was present in carboxyl groups.[2] For the supposedly surface-modified, commercially obtained NRCWE-047 and NRCWE-048, the total oxygen contents were lower than for the pristine NRCWE-046, indicating very low levels of surface functionalization by hydroxylation and carboxylation. The carbon black Printex 90 was included as a reference nanoparticle, to enable comparison of MWCNT-induced toxicity with a carbon-based nanoparticle with well-characterized toxicity.[35,41,51,52]

3.2 | Clinical findings

All mice were given a single intratracheal instillation at 8-9 weeks of age. In general, no severe clinical signs related to the administration of MWCNT were observed during one year of observation. A few mice had hair loss related to grooming and a few mice across groups experienced bites, including the control group. The 3 affected mice were euthanized and excluded from the study.

3.2.1 | Mouse weight

The average body-weight for all mice in the study, at instillation, was 18.6 ± 1.1 g. When the experiment was terminated one year later, the average body-weight was 27.7 ± 2.4 g. There was no difference between the growth curves of mice instilled with the different MWCNT or Printex 90, compared to vehicle-instilled mice.

3.2.2 | Open-field behaviour

There was no difference in behaviour between groups in the open-field test 11 months post-exposure, indicating no increased anxiety (data not shown).

3.3 | Histopathology

Figures 1 and 2 show representative overviews of haematoxylin and eosin (H&E) stained paraffin-embedded lung sections from mice exposed to the short and thin NM-403 (Figure 1A), long and thick NRCWE-006 (Figure 1B), vehicle control (Figure 2A) and surface-modified NRCWE-042 (Figure 2B) one year after exposure. MWCNT were generally observed as black aggregates in macrophages or granulomas (Figure 1Ai-ii, Figure 2Bii-iii and Figure S1A-B) for all MWCNT, except NM-401 and NRCWE-006. Only few NRCWE-006 aggregates were found in few exposed mice. With enhanced darkfield microscopy, MWCNT NRCWE-006 (Figure 1Bi-ii) and NM-401 (results not shown) were observed as single fibres throughout the lung and in liver (Figure 3).

Treatment-related pulmonary histopathological findings were evaluated and scored according to severity for granuloma formation, lymphocytic aggregates and macrophage infiltrates (Tables 2 and 3). More detailed scorings for each animal and additional statistical analysis are provided in Tables S3-S7.

Overall, the histopathological evaluation revealed that the two needlelike MWCNT (NRCWE-006 and NM-401) induced no histopathological changes compared to vehicle controls, whereas all thin and entangled MWCNT induced varying degrees of histopathological changes in terms of

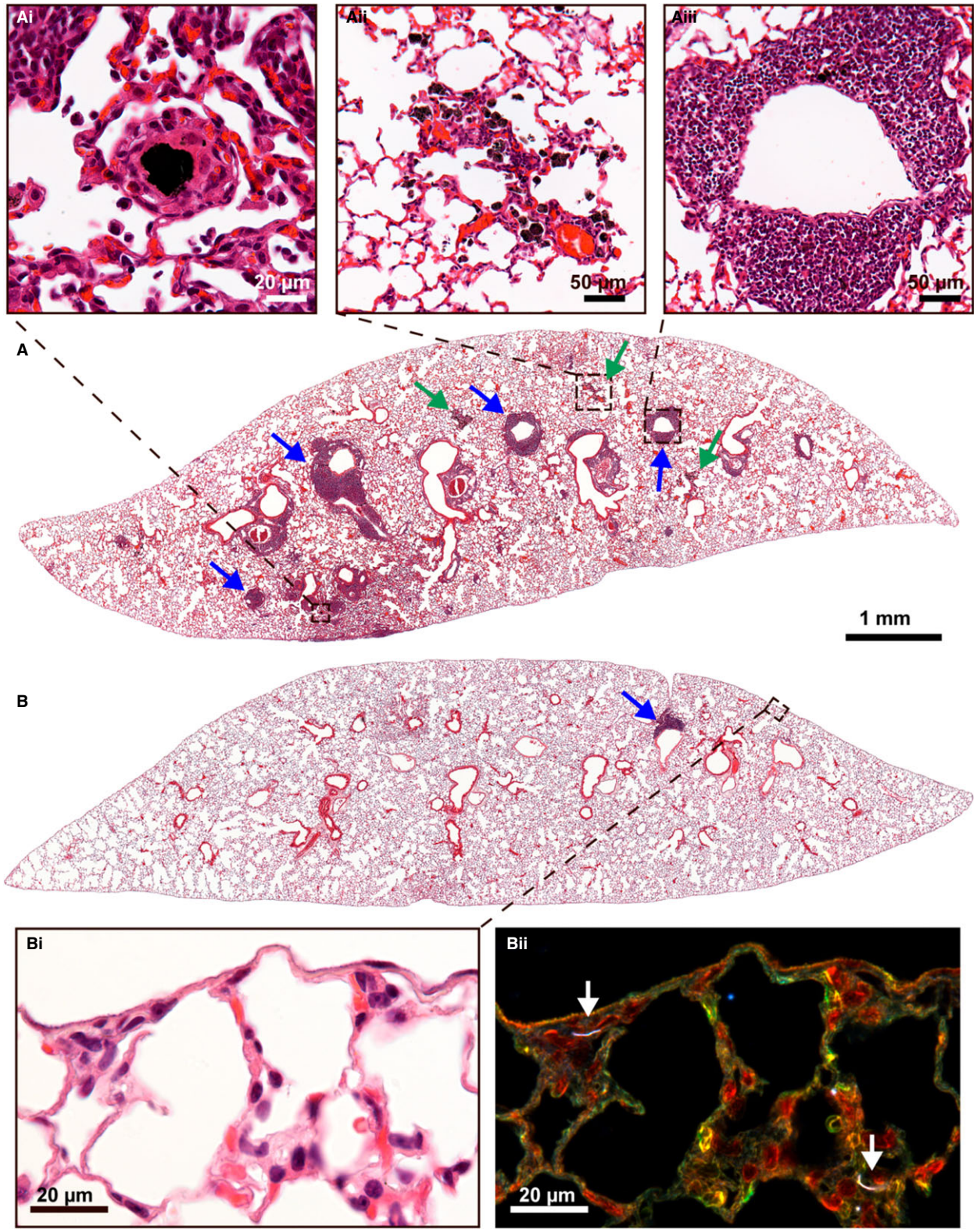

FIGURE 1 Lung sections from mice one year after instillation of 54 µg/animal of MWCNT: (A) NM-403 and (B) NRCWE-006 (Mitsui MWNT-7). The most common histopathological findings were foreign material granuloma (Ai), macrophage infiltrates (Aii, green arrows) and lymphocytic aggregates (Aiii, blue arrows). MWCNT were observed as black aggregates in granuloma (Ai) and in macrophages (Aii), except for NRCWE-006 (and NM-401, not shown) which were distributed as single fibres throughout the lung, detectable with enhanced darkfield (Bi-Bii, white arrows). H&E stain

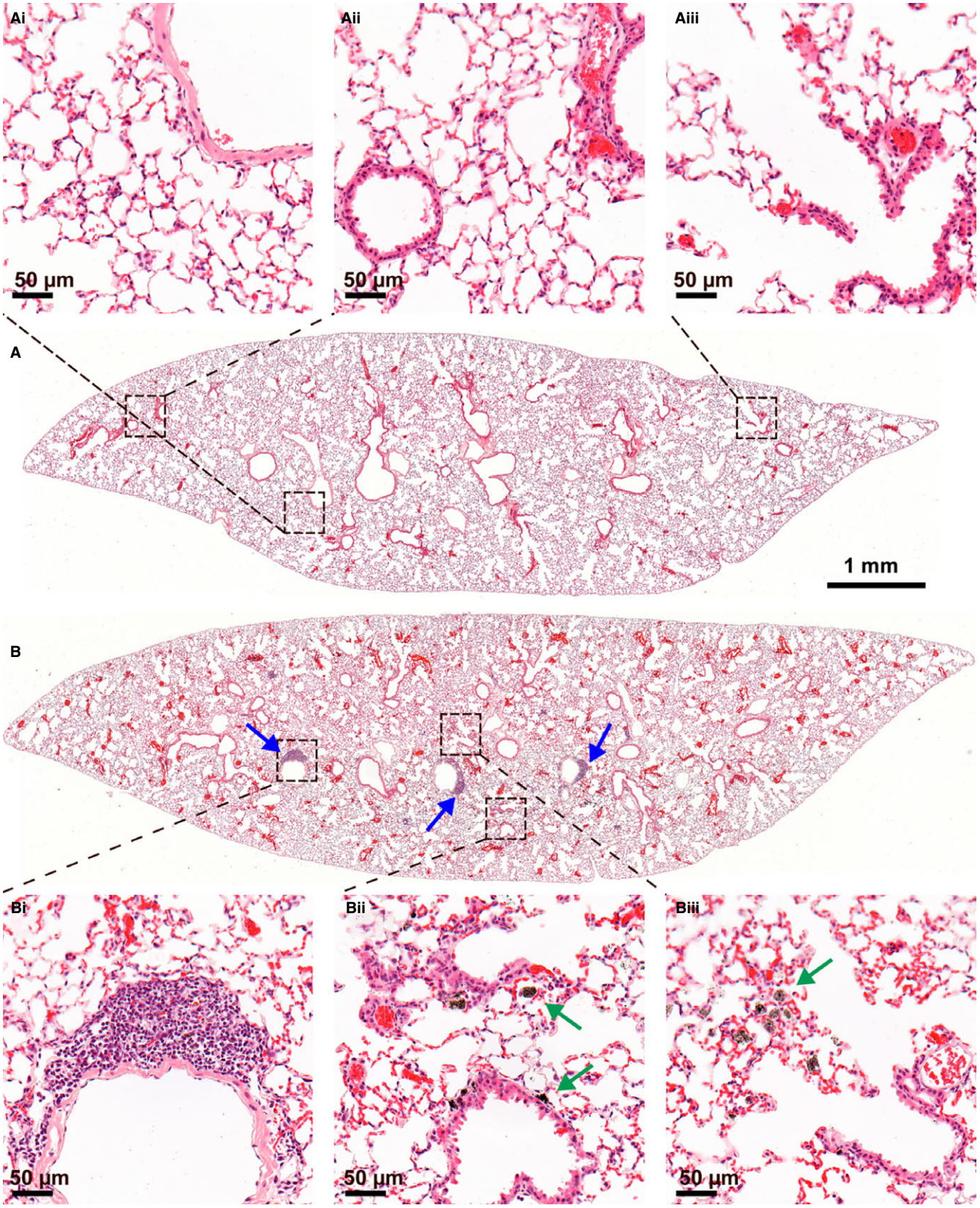

FIGURE 2 Lung sections one year after instillation of 0 (A) or 54 µg/animal (B) of MWCNT NRCWE-042: Vehicle control showed normal lung structure (Ai-Aiii). NRCWE-042 exposure gave lymphocytic aggregates (Bi, blue arrows). MWCNT were observed as black aggregates in macrophages (Bii, Biii, green arrows). H&E stain

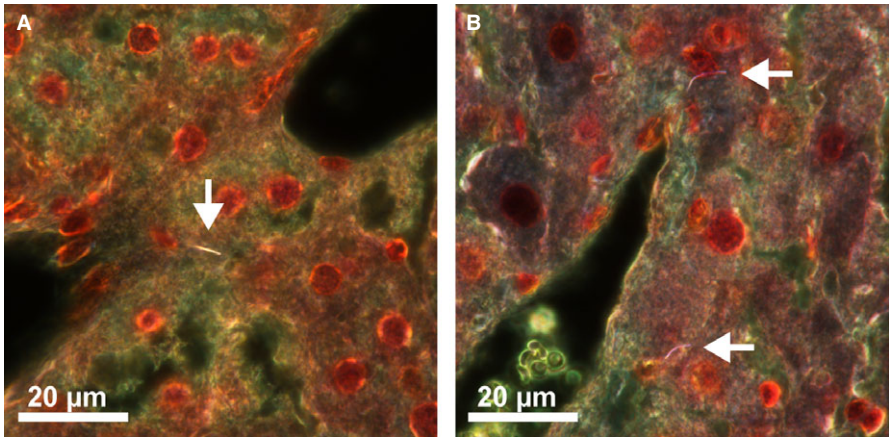

FIGURE 3 Enhanced darkfield of liver sections one year after instillation of MWCNT: NRCWE-006 (Mitsui MWNT-7) (A) and NM-401 (B). MWCNT were distributed as single fibres throughout the liver (white arrows). H&E stain

granuloma formation, lymphocytic aggregates and macrophage infiltrations.

3.3.1 | Granuloma formation

Granulomas were defined as foreign body granulomas with material surrounded entirely by adherent macrophages (Figure 1Ai and Figure S1A). The granulomas appeared rather inactive and often with a thin layer of macrophages. There was statistically significantly higher granuloma grading in groups instilled with NM-402, NM-403, NRCWE-040, -041, -046, -047, and -048 compared to the control group (Table 3 and Table S3). No foreign body granulomas were observed for NM-400, NM-401, NRCWE-006, Printex 90 or in vehicle controls.

3.3.2 | Lymphocytic aggregates

We observed lymphocytic aggregates of varying grading in all groups. This included the vehicle-exposed group, where low levels of lymphocytic aggregates were observed (Table 3 and Tables S5 and S7). The lymphocytic aggregates were often but not exclusively situated in perivascular or peribronchial areas. The majority of the cells were

TABLE 3 Mouse lung histopathology one year after instillation of 54 µg/animal of 11 different MWCNT

	Average histopathological grading			Total incidence per group	
MWCNT	Lymphocytic aggregates	Macrophage infiltrates	Granulomas	Interstitial fibrosis[e]	Tumours[e]
Vehicle control (N = 29)	1.3	0.1	0	0/29	0/29
NM-400 (N = 10)	2.2	0.3	0	1/10	1/10
NM-401 (N = 10)	1.9[a]	0.2	0	0/10	1/10
NM-402 (N = 10)	2.7***	0.8***	0.4*	0/10	0/10
NM-403 (N = 9)	3.7[b],***	1.2[d],***	1.44***	1/9	0/9
NRCWE-006 (N = 10)	1.2[c]	0.1	0	0/10	0/10
NRCWE-040 (N = 10)	3.3***	0.1	1.8***	0/10	0/10
NRCWE-041 (N = 10)	3.2***	0.3	1.1***	0/10	1/10
NRCWE-042 (N = 10)	2.2	0.5	0.2	0/10	0/10
NRCWE-046 (N = 10)	3.0***	0.5	0.5*	0/10	0/10
NRCWE-047 (N = 9)	3.7[b],***	0.6	1.33***	0/9	0/9
NRCWE-048 (N = 10)	3.4***	0.6*	1.5***	0/10	0/10
Printex 90 (N = 9)	2.6**	0.6*	0	0/9	0/9

Notes. Complete statistical comparison between MWCNT in Table S3-S7.

[a]Statistically significant ($P < 0.05$) lower lymphocyte grading compared to NM-403, NRCWE-040, -047 and -048. [b]Statistically significant higher lymphocyte grading compared to NM-400, NM-401, NRCWE-006 and -042. [c]Statistically significant lower lymphocyte grading compared to NM-402, NM-403, NRCWE-040, -041, -046, -047 and -048. [d]Statistically significant higher macrophage grading compared to NM-400, NM-401, NRCWE-006, -040 and -041. [e]No statistically significant difference in incidences of fibrosis or tumours between the groups.

*$P < 0.05$, **$P < 0.01$, ***$P < 0.001$ compared to vehicle control.

lymphocytes, with hyperchromatic nuclei and scant cytoplasm (Figure 1A,Aiii and Figure 2B,Bi).

Compared to vehicle-exposed controls, higher grading for lymphocytic aggregates were observed in mice instilled with NM-402, NM-403, NRCWE-040, -041, -046, -047, -048 and Printex 90 (Table 3). NM-401 induced a statistically significantly lower grading than NM-403, NRCWE-040, -047 and -048 (Table S7). NRCWE-006 induced statistically significantly lower grading compared to NM-402, NM-403, NRCWE-040, -041, -046, -047 and -048 (Table S7). NM-403 and NRCWE-047 induced statistically significantly higher lymphocyte grading compared to NM-400, NM-401, NRCWE-006 and -042 (Table S7).

3.3.3 | Macrophage infiltrates

Macrophage infiltration was observed in all groups including the vehicle control (Figure 1Aii and Figure S1B). The grading is shown in Table 3 and Table S4 and S6. NM-402, NM-403, NRCWE-048 and Printex 90 induced statistically significantly higher grading of macrophage infiltration compared to the vehicle control. NM-403 induced statistically significantly higher grading than NM-400, NM-401, NRCWE-006, -040 and -041.

3.3.4 | Other findings

Interstitial fibrosis occurred randomly in a few animals instilled with NM-400 (N = 1/10) and NM-403 (N = 1/9) (Figure 4A,B and Table 3). Adenomas of varying sizes were seen as single incidences in group NM-400, NM-401 and NRCWE-041 (Figure 4C and Table 3). All mice instilled with MWCNT, except NM-401 and NRCWE-006, displayed swollen and black mediastinal lymph nodes. The lymph nodes were examined, and MWCNT-like material was observed in histological sections by light microscopy. There were no significant histopathological changes detectable in the pleura, as assessed in histological samples from lungs and visceral pleura from the diaphragm and chest wall (results not shown).

3.4 | Genotoxicity in liver and spleen

Genotoxicity was measured by DNA strand breaks using the comet assay. Liver and spleen were chosen as target organs for systemic response, since these organs have been identified as target organs of translocated MWCNT.[17,53,54] Pulmonary exposure to NRCWE-040 increased levels of DNA strand breaks in liver tissue compared to vehicle controls ($P = 0.04$) (Figure S2). No significant changes were observed in spleen for any of the exposed groups (results not shown).

3.5 | Plasma serum amyloid A3

We have previously found a close correlation between neutrophil influx in BALF and pulmonary acute phase response in terms of Saa3 mRNA levels in lung tissue and SAA3 levels in plasma.[19,20,55,56] We therefore assessed plasma levels of SAA3 as a biomarker for inflammation. No difference was observed in the plasma levels of SAA3 (Figure S3).

3.6 | Multiple regression analyses

The pairwise association of physicochemical properties of MWCNT (BET surface area, diameter, length and content of elements Fe, Mn, Ni, Co, Mg and oxygen (OH)) was analysed using Pearson correlation analysis (Table S9). Two clusters of parameters were highly correlated: cluster 1 included BET surface area, diameter, length and Ni, and cluster 2 included Fe, Mn, Mg and Co (Mn, Mg and Co

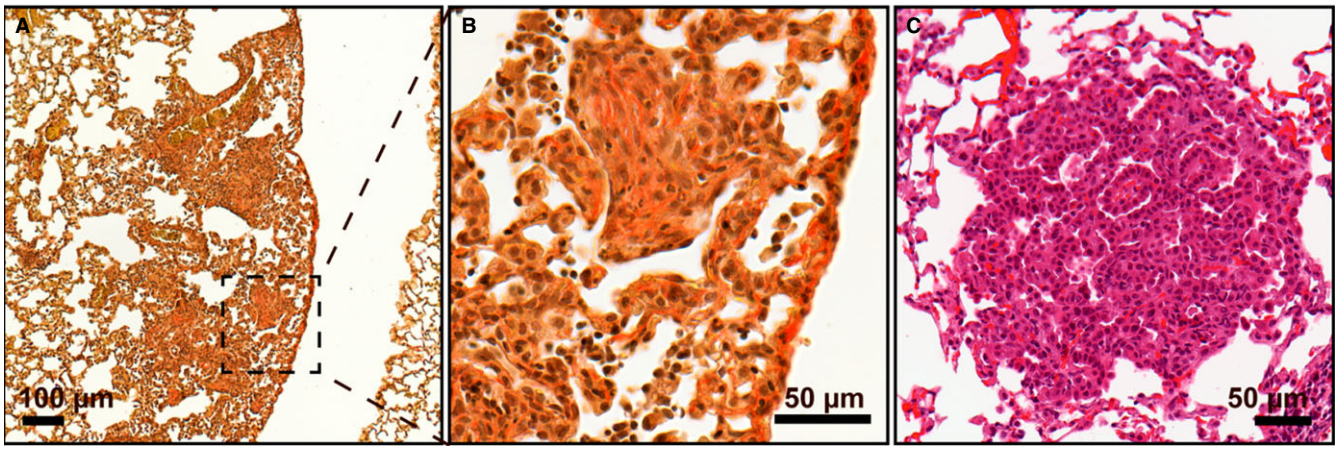

FIGURE 4 Rare histopathological findings: Fibrosis and tumours: (A,B) Immature connective tissue in NM-400 exposed mouse (Sirius Red–stained lung) and (C) adenoma in NM-401 exposed mouse (H&E-stained lung)

TABLE 4 Physicochemical parameters of MWCNT and their influence on histological outcome in the lung. Multiple regression (lymphocytic aggregates) and multiple logistic regression (macrophage infiltrations and granuloma formation) analyses

Exposure variable	Estimate	LowerCL	UpperCL	Probt
Lymphocytic aggregates				
Per doubling in OH	0.067	−0.036	0.17	0.197
Per doubling in **Fe**	**−0.124**	**−0.18**	**−0.07**	**<0.0001**
Per doubling in **diameter**	**−0.387**	**−0.602**	**−0.171**	**0.0006**
Exposure variable		**Estimate**	**SE**	**Probt ChiSq**
Macrophage infiltration				
Per doubling in OH		−0.02	0.13	0.876
Per doubling in Fe		−0.149	0.066	0.024
Per doubling in **diameter**		**−0.98**	**0.279**	**0.0004**
Granuloma formation				
Per doubling in OH		0.086	0.131	0.515
Per doubling in **Fe**		**−0.323**	**0.083**	**<0.0001**
Per doubling in **diameter**		**−1.031**	**0.303**	**0.0007**

Notes. OH: Hydroxyl content as regression variable for functionalization. Fe: Proxy variable for the highly correlated content of iron (Fe), manganese (Mn), magnesium (Mg) and cobalt (Co). Diameter: Proxy variable for the highly correlated diameter, length, BET surface area and nickel (Ni) content. Significantly predictive variables (Probt ≤ 0.01) are highlighted in bold. CL: confidence limit. SE: standard error.

correlated negatively with Fe). Log-transformed diameter was chosen as proxy variable for cluster 1, and log-transformed Fe content was chosen as proxy variable for cluster 2 in the multiple regression and multiple logistic regression analyses. Total oxygen content was an independent variable.

3.6.1 | Histological outcome

Selected physicochemical parameters (diameter, OH, and Fe) were related to the histological outcome in lung (Table 4). Increased diameter was a statistically significant positive predictor of reduced lymphocytic infiltration, reduced macrophage infiltration and reduced granuloma formation one year after exposure, meaning that a larger diameter resulted in less histological outcomes. The proxy variable for cluster 2, Fe content, was also a significant predictor of lymphocytic infiltration and granuloma formation, such that increasing Fe content predicted reduced lymphocytic infiltration and reduced granuloma formation. As a cluster effect, increasing Mn, Mg and Co content therefore resulted in increased lymphocytic infiltration and granuloma formation due to their negative correlation with Fe within the cluster. However, diameter (cluster 1) in general had a greater effect on the outcome than Fe (cluster 2). No effect of total oxygen content was observed. Multiple regression and logistic regression analyses using log-transformed length and log-transformed Mn as proxy variables for cluster 1 and 2, respectively, are presented in Tables S10-S12. Increased length significantly predicted less histological changes. However, both the effects of cluster 1 and 2 were dependent on the proxy variable of cluster 2. No statistically significant effects of either cluster were observed if Mn was selected as proxy variable, with the exception of a protective effect of increasing diameter on the macrophage infiltration.

Thus, the regression analysis identified some physicochemical properties predictive of the long-term histopathological changes in mouse lungs. Decreasing diameter induced more histopathological changes, as did decreasing Fe content (increasing Mn, Mg and Co content). Conversely, surface hydroxylation did not predict any histopathological changes.

3.6.2 | DNA strand breaks

Physicochemical parameters (diameter, OH and Fe) were analysed relative to DNA strand break levels in liver. No effects of any of the parameters were observed (Table S13). Multiple regression analyses using log-transformed length and log-transformed Mn as proxy variables for cluster 1 and cluster 2, respectively, were performed (Tables S14-S16). No significant effects were observed.

4 | DISCUSSION

We assessed lung histopathology, genotoxicity in liver and spleen, and the level of the acute phase protein SAA3 in the blood of mice one year after pulmonary exposure to 11 different MWCNT and Printex 90 by intratracheal exposure. The MWCNT varied in physicochemical properties, including physical dimensions, surface modifications and metal contents. We used multiple regression analyses to relate specific physicochemical properties to long-term toxicological effects.

Intratracheal instillation was chosen for pulmonary dosing. This technique ensures that the same dose is delivered to the lung for all MWCNT exposures, which is not necessarily the case in inhalation studies, since pulmonary deposition is determined by the aerodynamic size of MWCNT agglomerates and single fibres. We have previously shown that the used dispersion protocol and instillation technique gives a widespread distribution of particles throughout the lung,[57] also for MWCNT.[13] Instillation has the advantages that it requires less material and is more user-friendly, allowing for early screening without specialized inhalation

facilities and occupational health risks related to handling HARN materials. Studies comparing inhalation and instillation of MWCNT showed that both methods resulted in pulmonary inflammation, with inhalation being more potent at inducing inflammation.[58,59] It was recently shown that the global transcriptional pattern was similar in lungs from mice exposed to MWCNT by inhalation and aspiration, as well as for inhalation and intratracheal exposure to titanium dioxide particles.[32,36]

The dispersion state of MWCNT in the instillation media is important for both their toxicity and for distribution conformity across exposures. The MWCNT used in the present study have previously been characterized after dispersion in the instillation media (filtered Nanopure water with 2% mouse serum).[13,14] Briefly, dynamic light scattering analysis revealed that the MWCNT were generally well-dispersed. Exceptions were the needlelike NM-401 and NRCWE-006, probably due to limitations of the technique for measuring fibres.[2,13] SEM imaging of NRCWE-40, NRCWE-41, NRCWE-42, NRCWE-46, NRCWE-47 and NRCWE-48 also indicated that these materials were well-dispersed with some degrees of agglomeration in the instillation media at the dose used in the present study.[13] Dispersions of NM-400 and NM-401 have also previously been visualized with SEM.[14] In general, the more needlelike NM-401 appeared better dispersed and less agglomerated than the thinner and more curled up NM-400, although agglomerates were frequently observed for both materials.

In the present study, MWCNT were detected in the lungs one year after exposure to all MWCNT types, suggesting that all the studied MWCNT are biopersistent. However, whereas the short and entangled MWCNT types were observed as aggregates often enclosed in macrophages and granulomas, the two long, needlelike MWCNT (NM-401 and NRCWE-006) were observed as single fibres in the lung interstitium and in liver tissue (Figures 1 and 3). This is in concordance with our previous observations on MWCNT (NM-400 and NM-401) behaviour in the lung tissue 28 days after exposure using TEM.[60] Here, single NM-401 fibres were generally observed more often than NM-400 fibres, and the needlelike NM-401 appeared to escape vesicle enclosure more often compared to NM-400. Based on our visual evaluations (Figure 1), the needlelike MWCNT appeared to be cleared from the lungs to a greater extent than the thinner and entangled MWCNT. The initial difference in agglomeration state could in part explain this difference in clearance rate. Recently, Pauluhn and Rosenbruch (2015) showed that lung clearance was faster for single MWCNT fibres than for aggregates of the same MWCNT.[61] This indicates that the needlelike MWCNT more easily disassociate into smaller aggregates or singlet MWCNT, probably during breathing, whereas agglomerates of thin and entangled MWCNT, as observed in the present study, appear to both stay in agglomerates and to be more persistent in the lung.[62,63] In support of this, we detected MWCNT-like matter in mediastinal lymph nodes of all the thin MWCNT-exposed mice, whereas the mediastinal lymph nodes of mice exposed to the long, needlelike NM-401 and NRCWE-006 were not swollen and black one year post-exposure. These needlelike MWCNT likely cleared from the lungs at an earlier time-point, similar to what has been observed by others.[53,62] In concordance with this, we observed NM-401 fibres in the mediastinal lymph nodes at day 1, day 3 and day 90 post-exposure in another study in mice (KB Knudsen et al., unpublished results).

Exposure to 7 of the 11 MWCNT significantly increased the number of lymphocytic aggregates, and the same 7 of 11 MWCNT increased the incidence of granuloma compared to vehicle control mice (Table 3). Interestingly, these 7 MWCNT were all thin and entangled in physical appearance. In addition, NM-402, NM-403 and NRCWE-048 induced statistically significantly more macrophage infiltration than the vehicle control. We have previously reported histopathological findings indicative of inflammatory activity 28 and 90 days after pulmonary exposure to 10 different MWCNT of which 6 were also used in the present study.[13] When comparing the present data with histopathological changes observed 28 and 90 days post-exposure, levels of lymphocytic- and macrophage infiltration and granuloma formation were very similar for the thin and entangled MWCNT across time-points (Table S8). Also, similar levels of granuloma formations and inflammatory cell infiltrations were observed in sub-chronic inhalation studies in rats exposed to short and thin MWCNT.[63-65] Combined, the findings indicate that exposure to thin and entangled MWCNT induces a strong inflammatory response that persists to the chronic level.

The long and needlelike NM-401 and NRCWE-006 did not induce granuloma formation, lymphocyte aggregation or macrophage infiltration one year post-exposure. This is in contrast to other studies reporting dose-dependent macrophage infiltration and granulomatous tissue after pulmonary exposure to needlelike MWCNT of the same type as NRCWE-006 in 17-month and 2-year follow-up studies in mice and rats, respectively.[17,27,66] Not all animals in these studies were positive for the histopathological changes, and notably, only animals given a higher dose than the present study consistently showed pathological changes. In concordance with this, we have previously found small granulomatous changes along with inflammatory cells in the lungs of mice 28 days after receiving a three times higher dose than in the present study of the needlelike MWCNT.[14] We speculate that at a high pulmonary deposition of needlelike MWCNT granulomas are

formed, whereas in the present study, the relatively low dose of NRCWE-006 and NM-401 could have left the lung during the one-year follow-up, as also observed by Czarny et al[53] and Mercer et al.[15] This was supported by enhanced dark-field microscopy, with which the needlelike MWCNT were detected in liver tissue from NM-401- or NRCWE-006-exposed animals (Figure 3), suggesting translocation from lung to systemic circulation. Translocation of the thin and short MWCNT could not be assessed due to detection limitations.

In humans, chronic low-level inflammation caused by exposure to fibrous materials is a risk factor for lung malignancies and lung fibrosis.[67] A large proportion of *in vivo* studies with inhalation and instillation/aspiration of CNT reported fibrotic reactions.[26,68] However, in the present study, only few fibrotic lesions were observed in lungs across the MWCNT-exposed groups and none in pleura. The fibrotic lesions were rather focal and did not suggest a generalized or multifocal interstitial fibrosis as seen in, for example, asbestosis. Fibrosis formation after CNT exposure is dose-dependent,[25] and the dose used in the current study (54 μg/mouse, or approximately 2.9 mg/kg) is lower than the doses used in the *in vivo* studies reporting widespread fibrotic reactions.[68,69] Thus, it is likely that the dose used in the current study is too low for the evaluation of fibrogenicity of the MWCNT and further studies are required to fully address this point.

Studies have shown that thick and long needlelike MWCNT are carcinogenic,[17,27,28,30] whereas one thinner, shorter and entangled MWCNT was not carcinogenic in a 2-year rat study using intraperitoneal exposure.[29] This is in agreement with our previous studies, which linked increasing MWCNT diameter with increased genotoxicity, both in mice and murine cells.[2,13] In the current study, no size-dependent differences in carcinogenicity were observed, as only few, random tumours (n = 3) were observed in the lungs and none in pleura. This could be due to the administered dose, as tumour development has shown to be dose-dependent.[17] In addition, the group size and follow-up time in the present study were not designed for evaluating tumour formation. It has been suggested that granulomas are protective structures.[70] Following this suggestion, long and needlelike MWCNT could be more carcinogenic than the smaller entangled type, as they disperse in the lung tissue over time and avoid encapsulation in protective granulomas.

We did not assess pulmonary genotoxicity in the current study, because DNA strand breaks are assessed in cryo-preserved tissue, whereas paraffin-embedded tissue is required for the histopathological evaluation, which is the main focus of the current study. Instead, genotoxicity was assessed in the main target organs for translocated MWCNT, liver and spleen. We have recently shown that carbon black-induced genotoxicity in liver is caused by translocation of particles.[71] In the current study, only one MWCNT, NRCWE-040, induced DNA strand breaks in liver. The observed significantly increased DNA strand break levels are similar to the increases in DNA strand break levels observed in liver tissue 28 days after pulmonary exposure to nano carbon black, and in lung tissue 28 days after pulmonary exposure to NM-400 and NM-401.[14,35] We were unable to identify physicochemical properties important for MWCNT-induced DNA damage in the liver after pulmonary exposure.

Physicochemical properties were related to the observed pulmonary histological changes in multiple regression and multiple logistic regression analyses. MWCNT diameter, length and BET surface area were highly correlated, and inseparable in the statistical analyses. Diameter was a statistically significant predictor of the pulmonary histological outcome when used as the proxy variable for cluster 1 (diameter, length, BET surface area and Ni), indicating that thicker and needlelike MWCNT induce less histological changes compared to their thinner counterparts. This is in line with our general observations showing no significant pulmonary histopathological changes after exposure to the needlelike MWCNT. Surface hydroxylation did not appear to impact pulmonary histopathology. Fe content as proxy variable for cluster 2 (Fe, Mn, Mg and Co) appeared to be protective of the histological changes; however, as Fe is a known generator of reactive oxygen species (ROS), this protective effect was probably caused by the negative correlation with Mn, Mg and Co. Mn has been related to adverse pulmonary effects,[72,73] it is, however, unlikely that the low amounts of Mn and Mg present in the MWCNT are determinants of histological changes. Lastly, Co exposure has been reported to result in adverse pulmonary effects[74] and has been classified as possibly carcinogenic to humans.[75] Co content could therefore be important for MWCNT-induced lymphocytic infiltration and granuloma formation. Although, these statistical analyses provide important insight into long-term MWCNT-induced toxicity and suggest possible toxicity-driving properties, the end is far from reached. Further studies using larger arrays of MWCNT, with a wide span of physicochemical properties and doses, are required to continue towards identification of toxicity-inducing physicochemical properties. Such identification could pave the way for the construction of MWCNT, which contain their positive qualities while also being safe for humans to use.

In conclusion, large variation in induced pulmonary histopathological changes was observed one year after pulmonary exposure to 11 MWCNT with different physicochemical properties. We were able to detect all MWCNT types in the lung tissue of the exposed mice, suggesting that these nanomaterials are biopersistent one year after

exposure. However, the two long and thick MWCNT were almost exclusively observed as single fibres. The thin and entangled MWCNT were observed as agglomerates and were the only type that induced granuloma formation and lymphocytic aggregates in lungs. Regression analyses confirmed diameter as predictor of histopathological changes. Same analyses also identified Co content as a possible predictor of lymphocytic infiltration and granuloma formation. These results could be a possible first step towards designing MWCNT that induce less long-term lymphocytic infiltration and granuloma formation.

ACKNOWLEDGEMENTS

Technical assistance from Michael Guldbrandsen, Eva Terrida, Lourdes Pedersen, Elzbieta Christiansen, Anne-Karin Asp, Zdenka Orabi Kyjovska, Noor Irmam and Sauli Savukoski is greatly appreciated. The authors also greatly appreciate the statistical support from Birthe Lykke Thomsen and thank Dr. Fiona Murphy from University of Edinburgh, Scotland, for introducing the recovery of chest wall and diaphragm for histological analysis.

ETHICS APPROVAL

All animal procedures complied with the EC Directive 86/609/EEC and Danish law regulating experiments with animals (The Danish Ministry of Justice, Animal Experiments Inspectorate, permission 2006/561-1123). All animal procedures are approved by the local Animal Experimentation Committee. See Appendix S1 for details.

CONFLICT OF INTEREST

The authors report no conflict of interests.

REFERENCES

1. Donaldson K, Murphy FA, Duffin R, Poland CA. Asbestos, carbon nanotubes and the pleural mesothelium: a review of the hypothesis regarding the role of long fibre retention in the parietal pleura, inflammation and mesothelioma. *Part Fibre Toxicol*. 2010;7:5.
2. Jackson P, Kling K, Jensen KA, et al. Characterization of genotoxic response to 15 multiwalled carbon nanotubes with variable physicochemical properties including surface functionalizations in the FE1-Muta(TM) mouse lung epithelial cell line. *Environ Mol Mutagen*. 2015;56:183-203.
3. Beg S, Rizwan M, Sheikh AM, Hasnain MS, Anwer K, Kohli K. Advancement in carbon nanotubes: basics, biomedical applications and toxicity. *J Pharm Pharmacol*. 2011;63:141-163.
4. Klumpp C, Kostarelos K, Prato M, Bianco A. Functionalized carbon nanotubes as emerging nanovectors for the delivery of therapeutics. *Biochim Biophys Acta*. 2006;1758:404-412.
5. Shvedova AA, Yanamala N, Kisin ER, Khailullin TO, Birch ME, Fatkhutdinova LM. Integrated analysis of dysregulated ncRNA and mRNA expression profiles in humans exposed to carbon nanotubes. *PLoS ONE*. 2016;11:e0150628.
6. Muller J, Huaux F, Moreau N, et al. Respiratory toxicity of multi-wall carbon nanotubes. *Toxicol Appl Pharmacol*. 2005;207:221-231.
7. Dong J, Porter DW, Batteli LA, Wolfarth MG, Richardson DL, Ma Q. Pathologic and molecular profiling of rapid-onset fibrosis and inflammation induced by multi-walled carbon nanotubes. *Arch Toxicol*. 2014;89:621-633.
8. Hamilton RF Jr, Wu Z, Mitra S, Shaw PK, Holian A. Effect of MWCNT size, carboxylation, and purification on in vitro and in vivo toxicity, inflammation and lung pathology. *Part Fibre Toxicol*. 2013;10:57.
9. Porter DW, Wu N, Hubbs AF, et al. Differential mouse pulmonary dose and time course responses to titanium dioxide nanospheres and nanobelts. *Toxicol Sci*. 2013;131:179-193.
10. Murphy FA, Poland CA, Duffin R, et al. Length-dependent retention of carbon nanotubes in the pleural space of mice initiates sustained inflammation and progressive fibrosis on the parietal pleura. *Am J Pathol*. 2011;178:2587-2600.
11. Rydman EM, Ilves M, Koivisto AJ, et al. Inhalation of rod-like carbon nanotubes causes unconventional allergic airway inflammation. *Part Fibre Toxicol*. 2014;11:48.
12. Poland CA, Duffin R, Kinloch I, et al. Carbon nanotubes introduced into the abdominal cavity of mice show asbestos-like pathogenicity in a pilot study. *Nat Nanotechnol*. 2008;3:423-428.
13. Poulsen SS, Jackson P, Kling K, et al. Multi-walled carbon nanotube physicochemical properties predict pulmonary inflammation and genotoxicity. *Nanotoxicology*. 2016;10:1263-1275.
14. Poulsen SS, Saber AT, Williams A, et al. MWCNTs of different physicochemical properties cause similar inflammatory responses, but differences in transcriptional and histological markers of fibrosis in mouse lungs. *Toxicol Appl Pharmacol*. 2015;284:16-32.
15. Mercer RR, Hubbs AF, Scabilloni JF, et al. Pulmonary fibrotic response to aspiration of multi-walled carbon nanotubes. *Part Fibre Toxicol*. 2011;8:21.
16. Kasai T, Umeda Y, Ohnishi M, et al. Thirteen-week study of toxicity of fiber-like multi-walled carbon nanotubes with whole-body inhalation exposure in rats. *Nanotoxicology*. 2014;9:1-10.
17. Kasai T, Umeda Y, Ohnishi M, et al. Lung carcinogenicity of inhaled multi-walled carbon nanotube in rats. *Part Fibre Toxicol*. 2016;13:53.
18. Chen T, Nie H, Gao X, et al. Epithelial-mesenchymal transition involved in pulmonary fibrosis induced by multi-walled carbon nanotubes via TGF-beta/Smad signaling pathway. *Toxicol Lett*. 2014;226:150-162.
19. Poulsen SS, Knudsen KB, Jackson P, et al. Multi-walled carbon nanotube-physicochemical properties predict the systemic acute phase response following pulmonary exposure in mice. *PLoS ONE*. 2017;5:e0174167.
20. Poulsen SS, Saber AT, Mortensen A, et al. Changes in cholesterol homeostasis and acute phase response link pulmonary exposure to multi-walled carbon nanotubes to risk of cardiovascular disease. *Toxicol Appl Pharmacol*. 2015;283:210-222.
21. Kim JE, Lee S, Lee AY, Seo HW, Chae C, Cho MH. Intratracheal exposure to multi-walled carbon nanotubes induces a nonalcoholic steatohepatitis-like phenotype in C57BL/6J mice. *Nanotoxicology*. 2015;9:613-623.

22. Cao Y, Jacobsen NR, Danielsen PH, et al. Vascular effects of multiwalled carbon nanotubes in dyslipidemic ApoE-/- mice and cultured endothelial cells. *Toxicol Sci*. 2014;138:104-116.
23. Christophersen DV, Jacobsen NR, Andersen MH, et al. Cardiovascular health effects of oral and pulmonary exposure to multi-walled carbon nanotubes in ApoE-deficient mice. *Toxicology*. 2016;371:29-40.
24. Ma-Hock L, Treumann S, Strauss V, et al. Inhalation toxicity of multiwall carbon nanotubes in rats exposed for 3 months. *Toxicol Sci*. 2009;112:468-481.
25. Pauluhn J. Multi-walled carbon nanotubes (Baytubes): approach for derivation of occupational exposure limit. *Regul Toxicol Pharmacol*. 2010;57:78-89.
26. Pothmann D, Simar S, Schuler D, et al. Lung inflammation and lack of genotoxicity in the comet and micronucleus assays of industrial multiwalled carbon nanotubes Graphistrength((c)) C100 after a 90-day nose-only inhalation exposure of rats. *Part Fibre Toxicol*. 2015;12:21.
27. Suzui M, Futakuchi M, Fukamachi K, et al. Multiwalled carbon nanotubes intratracheally instilled into the rat lung induce development of pleural malignant mesothelioma and lung tumors. *Cancer Sci*. 2016;107:924-935.
28. Rittinghausen S, Hackbarth A, Creutzenberg O, et al. The carcinogenic effect of various multi-walled carbon nanotubes (MWCNTs) after intraperitoneal injection in rats. *Part Fibre Toxicol*. 2014;11:59.
29. Muller J, Delos M, Panin N, Rabolli V, Huaux F, Lison D. Absence of carcinogenic response to multiwall carbon nanotubes in a 2-year bioassay in the peritoneal cavity of the rat. *Toxicol Sci*. 2009;110:442-448.
30. Grosse Y, Loomis D, Guyton KZ, et al. Carcinogenicity of fluoro-edenite, silicon carbide fibres and whiskers, and carbon nanotubes. *Lancet Oncol*. 2014;15:1427-1428.
31. Schmid O, Cassee FR. On the pivotal role of dose for particle toxicology and risk assessment: exposure is a poor surrogate for delivered dose. *Part Fibre Toxicol*. 2017;14:52.
32. Kinaret P, Ilves M, Fortino V, et al. Inhalation and oropharyngeal aspiration exposure to rod-like carbon nanotubes induce similar airway inflammation and biological responses in mouse lungs. *ACS Nano*. 2017;11:291-303.
33. Palomaki J, Valimaki E, Sund J, et al. Long, needle-like carbon nanotubes and asbestos activate the NLRP3 inflammasome through a similar mechanism. *ACS Nano*. 2011;5:6861-6870.
34. Shvedova AA, Kisin E, Murray AR, et al. Inhalation vs. aspiration of single-walled carbon nanotubes in C57BL/6 mice: inflammation, fibrosis, oxidative stress, and mutagenesis. *Am J Physiol Lung Cell Mol Physiol*. 2008;295:L552-L565.
35. Bourdon JA, Saber AT, Jacobsen NR, et al. Carbon black nanoparticle instillation induces sustained inflammation and genotoxicity in mouse lung and liver. *Part Fibre Toxicol*. 2012;9:5.
36. Husain M, Saber AT, Guo C, et al. Pulmonary instillation of low doses of titanium dioxide nanoparticles in mice leads to particle retention and gene expression changes in the absence of inflammation. *Toxicol Appl Pharmacol*. 2013;269:250-262.
37. Saber AT, Jacobsen NR, Mortensen A, et al. Nanotitanium dioxide toxicity in mouse lung is reduced in sanding dust from paint. *Part Fibre Toxicol*. 2012;9:4.
38. Saber AT, Koponen IK, Jensen KA, et al. Inflammatory and genotoxic effects of sanding dust generated from nanoparticle-containing paints and lacquers. *Nanotoxicology*. 2012;6:776-788.
39. NIOSH. Current intelligence bulletin 65: Occupational Exposure to Carbon Nanotubes and Nanofibers. 2013;2013:145.
40. Baisch BL, Corson NM, Wade-Mercer P, et al. Equivalent titanium dioxide nanoparticle deposition by intratracheal instillation and whole body inhalation: the effect of dose rate on acute respiratory tract inflammation. *Part Fibre Toxicol*. 2014;11:5.
41. Kyjovska ZO, Jacobsen NR, Saber AT, et al. DNA damage following pulmonary exposure by instillation to low doses of carbon black (Printex 90) nanoparticles in mice. *Environ Mol Mutagen*. 2015;56:41-49.
42. Jackson P, Hougaard KS, Vogel U, et al. Exposure of pregnant mice to carbon black by intratracheal instillation: toxicogenomic effects in dams and offspring. *Mutat Res*. 2012;745:73-83.
43. Jackson P, Hougaard KS, Boisen AM, et al. Pulmonary exposure to carbon black by inhalation or instillation in pregnant mice: effects on liver DNA strand breaks in dams and offspring. *Nanotoxicology*. 2012;6:486-500.
44. Bourdon JA, Halappanavar S, Saber AT, et al. Hepatic and pulmonary toxicogenomic profiles in mice intratracheally instilled with carbon black nanoparticles reveal pulmonary inflammation, acute phase response, and alterations in lipid homeostasis. *Toxicol Sci*. 2012;127:474-484.
45. Saber AT, Jensen KA, Jacobsen NR, et al. Inflammatory and genotoxic effects of nanoparticles designed for inclusion in paints and lacquers. *Nanotoxicology*. 2012;6:453-471.
46. Jacobsen NR, Stoeger T, van den Brule S, et al. Acute and subacute pulmonary toxicity and mortality in mice after intratracheal instillation of ZnO nanoparticles in three laboratories. *Food Chem Toxicol*. 2015;85:84-95.
47. Jackson P, Vogel U, Wallin H, Hougaard KS. Prenatal exposure to carbon black (printex 90): effects on sexual development and neurofunction. *Basic Clin Pharmacol Toxicol*. 2011;109:434-437.
48. Schneider CA, Rasband WS, Eliceiri KW. NIH Image to ImageJ: 25 years of image analysis. *Nat Methods*. 2012;9:671-675.
49. Thevenaz P, Unser M. User-friendly semiautomated assembly of accurate image mosaics in microscopy. *Microsc Res Tech*. 2007;70:135-146.
50. Jackson P, Pedersen LM, Kyjovska ZO, et al. Validation of freezing tissues and cells for analysis of DNA strand break levels by comet assay. *Mutagenesis*. 2013;28:699-707.
51. Bengtson S, Knudsen KB, Kyjovska ZO, et al. Differences in inflammation and acute phase response but similar genotoxicity in mice following pulmonary exposure to graphene oxide and reduced graphene oxide. *PLoS ONE*. 2017;12:e0178355.
52. Jacobsen NR, Clausen PA. Carbon black nanoparticles and other problematic constituents of black ink and their potential to harm tattooed humans. *Curr Probl Dermatol*. 2015;48:170-175.
53. Czarny B, Georgin D, Berthon F, et al. Carbon nanotube translocation to distant organs after pulmonary exposure: insights from in situ (14)c-radiolabeling and tissue radioimaging. *ACS Nano*. 2014;8:5715-5724.
54. Mercer RR, Scabilloni JF, Hubbs AF, et al. Extrapulmonary transport of MWCNT following inhalation exposure. *Part Fibre Toxicol*. 2013;10:38.
55. Saber AT, Jacobsen NR, Jackson P, et al. Particle-induced pulmonary acute phase response may be the causal link between

particle inhalation and cardiovascular disease. *Wiley Interdiscip Rev Nanomed Nanobiotechnol*. 2014;6:517-531.
56. Saber AT, Lamson JS, Jacobsen NR, et al. Particle-induced pulmonary acute phase response correlates with neutrophil influx linking inhaled particles and cardiovascular risk. *PLoS ONE*. 2013;8:e69020.
57. Mikkelsen L, Sheykhzade M, Jensen KA, et al. Modest effect on plaque progression and vasodilatory function in atherosclerosis-prone mice exposed to nanosized TiO(2). *Part Fibre Toxicol*. 2011;8:32.
58. Morimoto Y, Hirohashi M, Ogami A, et al. Pulmonary toxicity of well-dispersed multi-wall carbon nanotubes following inhalation and intratracheal instillation. *Nanotoxicology*. 2012;6:587-599.
59. Porter DW, Hubbs AF, Chen BT, et al. Acute pulmonary dose-responses to inhaled multi-walled carbon nanotubes. *Nanotoxicology*. 2013;7:1179-1194.
60. Køibler C, Poulsen SS, Saber AT, et al. Time-dependent subcellular distribution and effects of carbon nanotubes in lungs of mice. *PLoS ONE*. 2015;10:e0116481.
61. Pauluhn J, Rosenbruch M. Lung burdens and kinetics of multi-walled carbon nanotubes (Baytubes) are highly dependent on the disaggregation of aerosolized MWCNT. *Nanotoxicology*. 2015;9:242-252.
62. Mercer RR, Scabilloni JF, Hubbs AF, et al. Distribution and fibrotic response following inhalation exposure to multi-walled carbon nanotubes. *Part Fibre Toxicol*. 2013;10:33.
63. Xu J, Alexander DB, Futakuchi M, et al. Size- and shape-dependent pleural translocation, deposition, fibrogenesis, and mesothelial proliferation by multiwalled carbon nanotubes. *Cancer Sci*. 2014;105:763-769.
64. Pauluhn J. Subchronic 13-week inhalation exposure of rats to multiwalled carbon nanotubes: toxic effects are determined by density of agglomerate structures, not fibrillar structures. *Toxicol Sci*. 2010;113:226-242.
65. Xu J, Futakuchi M, Shimizu H, et al. Multi-walled carbon nanotubes translocate into the pleural cavity and induce visceral mesothelial proliferation in rats. *Cancer Sci*. 2012;103:2045-2050.
66. Sargent LM, Porter DW, Staska LM, et al. Promotion of lung adenocarcinoma following inhalation exposure to multi-walled carbon nanotubes. *Part Fibre Toxicol*. 2014;11:3.
67. Mossman BT, Churg A. Mechanisms in the pathogenesis of asbestosis and silicosis. *Am J Respir Crit Care Med*. 1998;157:1666-1680.
68. Vietti G, Lison D, van den Brule S. Mechanisms of lung fibrosis induced by carbon nanotubes: towards an Adverse Outcome Pathway (AOP). *Part Fibre Toxicol*. 2016;13:11.
69. Labib S, Williams A, Yauk CL, et al. Nano-risk Science: application of toxicogenomics in an adverse outcome pathway framework for risk assessment of multi-walled carbon nanotubes. *Part Fibre Toxicol*. 2016;13:15.
70. Majno G, Joris I. *Cells, Tissues and Disease*, 2nd edn. Oxford, UK: Oxford University Press; 2004.
71. Modrzynska J, Berthing T, Ravn-Haren G, et al. Primary genotoxicity in the liver following pulmonary exposure to carbon black nanoparticles in mice. *Part Fibre Toxicol*. 2018;15:2.
72. Bowman AB, Kwakye GF, Herrero HE, Aschner M. Role of manganese in neurodegenerative diseases. *J Trace Elem Med Biol*. 2011;25:191-203.
73. Crossgrove J, Zheng W. Manganese toxicity upon overexposure. *NMR Biomed*. 2004;17:544-553.
74. NIOSH. Occupational Safety and Health Guideline for Cobalt; 1978.
75. IARC. IARC working group on the evaluation of carcinogenic risks to humans: Cobalt in Hard Metals and Cobalt Sulfate, Gallium Arsenide, Indium Phosphide and Vanadium Pentoxide. *IARC Monogr Eval Carcinog Risks Hum*. 2006.86:1-294

SUPPORTING INFORMATION

Additional supporting information may be found online in the Supporting Information section at the end of the article.

How to cite this article: Knudsen KB, Berthing T, Jackson P, et al. Physicochemical predictors of Multi-Walled Carbon Nanotube–induced pulmonary histopathology and toxicity one year after pulmonary deposition of 11 different Multi-Walled Carbon Nanotubes in mice. *Basic Clin Pharmacol Toxicol*. 2019;124:211–227. https://doi.org/10.1111/bcpt.13119